



Study on the double micro-mesh gaseous structure (DMM) as a photon detector

Zhiyong Zhang, Binbin Qi, Ming Shao^{*}, Jianxin Feng, Xu Wang, Chengming Liu, Jianbei Liu, Yi Zhou, Daojin Hong, You Lv, Guofeng Song, Wenhao You

State Key Laboratory of Particle Detection and Electronics, University of Science and Technology of China, Hefei 230026, China
Department of Modern Physics, University of Science and Technology of China, Hefei 230026, China

ARTICLE INFO

Keywords:

Gaseous photomultiplier
Micromegas
Double mesh
Single electron
Ion-backflow
Gas gain

ABSTRACT

Application of micro-pattern gaseous detectors (MPGD) to photon detection has been widely investigated over the past decades. A double micro-mesh gaseous structure (DMM) prototype is developed with a thermal bonding technique for this application. Excellent performance for detecting single photon has been demonstrated in various tests with X-ray and ultra-violet (UV) laser light. The gain of the DMM prototype can reach up to $>10^6$ for single electrons while maintaining a very low ion-backflow (IBF) ratio down to $<0.05\%$, showing good potential to serve as the photon detector in Cherenkov light detection, as well as for other applications, e.g. TPC readout, where a very low level of IBF is needed. The method to further suppress the IBF of DMM is discussed, and verified by simulation and experimental studies.

1. Introduction

Gaseous photomultipliers (GPMs) using micro-pattern gas detectors (MPGDs) have been widely studied in the last decades, owing to their advantages such as large effective area with low cost, good spatial and time resolution, and high magnetic field resistance [1,2]. However, improvements are still needed, low. It has been suggested that mesh-type MPGDs (e.g. Micro-mesh gaseous especially to increase the gain of GPM while keeping the ion back-flow (IBF) structure, Micromegas) have a better IBF suppression capability than hole-type ones (such as usual or thick gas electron multiplier, GEM/THGEM) [3]. In this work, a double micro-mesh gaseous structure (DMM) [4,5] in which another mesh is added on top of a typical Micromegas is introduced, in order to further enhance the benefit from single layer Micromegas. With such a structure, a very high gas gain can be obtained through the cascading avalanche amplification; meanwhile the IBF can be strongly suppressed with proper electric potential configuration on the two mesh layers. In addition to GPM application, the DMM provides a new option for other applications requiring very low IBF [6–8].

2. Design and fabrication of DMM

The schematic view of a DMM is illustrated in Fig. 1. Two stacked micro-meshes divide the structure into three regions, namely the drift region, the pre-amplification (PA) region and the secondary amplification (SA) region. The PA region between 2 meshes is $\sim 240 \mu\text{m}$ thick, and the SA region is $\sim 120 \mu\text{m}$ thick, formed by the bottom mesh and the

anode. During normal operation, the strong electric fields in the PA and SA regions provide high gas gain and fast collection of the avalanche charges.

An assembled DMM prototype is also shown in Fig. 1. This detector is produced with a thermal bonding technique [9,10]. Thermal bonding spacers, round pillars of 1 mm in diameter, are regularly set on a readout PCB with a pitch of 1 cm to keep an appropriate avalanche gap of $\sim 120 \mu\text{m}$ which is defined by the spacer height after thermo-compression bonding with a hot roller. The PA gap of $\sim 240 \mu\text{m}$ is similarly determined by another layer of spacers, stacking on top of the first layer. The SA and PA meshes used are made of 500 LPI stainless steel, $27 \mu\text{m}$ thick with a $\sim 40\%$ optical transparency. Both layers of meshes are stretched with a tension of $\sim 20 \text{ N/cm}$ to ensure good uniformity. A series of DMMs are produced with this method, while for this work only a small prototype with an active area of $2.5 \times 2.5 \text{ cm}^2$ is studied.

3. Performance of DMM

3.1. Gas gain

The test on the DMM prototype is carried out at a test setup equipped a charge sensitive pre-amplifier, a shaping main amplifier and a multichannel analyzer (MCA). A ^{55}Fe source is used and the working gas is a mixture of 93% Argon and 7% CO_2 .

^{*} Corresponding author at: Department of Modern Physics, University of Science and Technology of China, Hefei 230026, China.
E-mail address: swing@ustc.edu.cn (M. Shao).

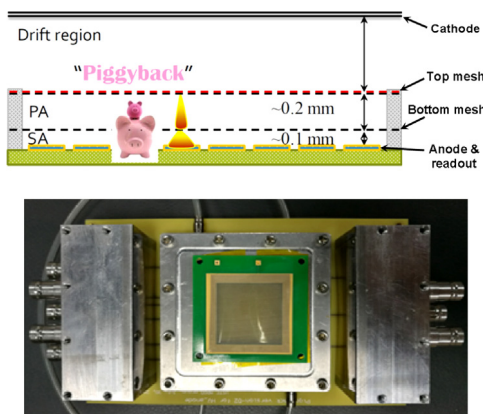


Fig. 1. The schematic structure and assembled prototype of DMM.

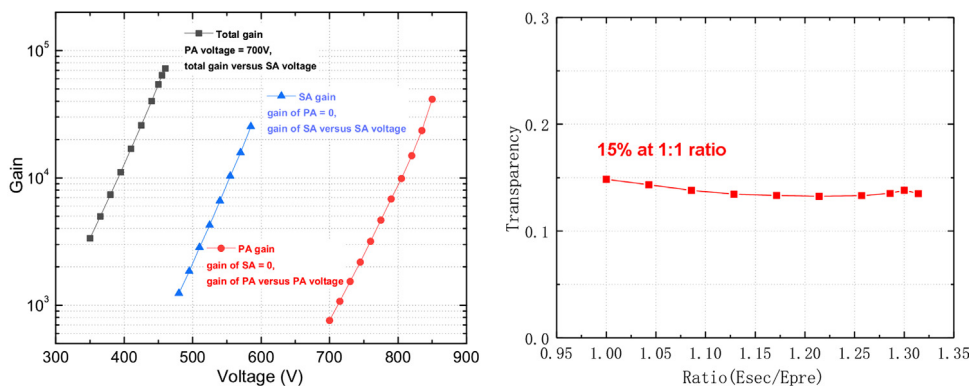


Fig. 2. (left) The total, single PA and single SA gains of the DMM prototype. (right) The electron transparency between the PA and SA regions. (For interpretation of the references to color in this figure legend, the reader is referred to the web version of this article.)

As the first step, the PA and SA regions of the prototype are tested individually in order to better understand the amplification and transition of charges in DMM. The voltages on the cathode and two meshes are configured in ways that the DMM prototype operated as a typical Micromegas with a single amplification stage. For the single PA mode, the electron transparency increases with the ratio of electric fields between the PA and drift regions (E_{PA}/E_{drift}), and saturates when E_{PA}/E_{drift} is over 200. A maximum gas gain up to 4×10^4 is achieved before spark sets in. For the single SA mode similar results are obtained, with a maximum achievable gain of $>2 \times 10^4$.

The DMM prototype is then tested at its normal operation mode, with successive charge amplification in the PA and SA regions. Fig. 2 (left) shows the total gain of DMM, as well as the single SA and single PA results. The data points in Fig. 2 (left) are the single PA gain as a function of PA voltage (red dots), the single SA gain as a function of SA voltage (blue triangles), and the total gain as a function of the SA voltage with a fixed PA voltage of 700 V (black rectangles). The total gain can reach up to 7×10^4 , corresponding to a total amount of more than 10^7 electrons (and ions) produced in the SA region, considering the >200 primary ionization electrons produced by the 5.9 keV ^{55}Fe X-ray. The maximum total gain is limited by the large amount of charge produced in the SA gas gap which has a high probability of triggering a spark.

The electron transparency from PA to SA is shown in Fig. 2 (right). It is simply estimated by the formula: Total gain = Single PA gain \times Transparency \times Single SA gain. When the electric fields are similar in the PA and SA regions, i.e. $E_{PA}/E_{SA} \sim 1$, the electron transparency is about 15%.

An ultra-violet (UV) laser COMPILER UPGRADE-400 [11] is used to test the single photo-electron response of the DMM prototype. The UV light from the laser passes through a 3 mm thick quartz window and

interacted with a ~ 10 nm thick Aluminum cathode coated on the inner surface of the window, producing photoelectrons as shown in Fig. 3 (left). To ensure that the measurement is dominated by single electron response, the laser (400 Hz pulse rate) is attenuated so that the DMM only measures signal at a few Hz rate, which means most of the laser pulse are too weak to be detected, and the peak and width of the ADC spectra stay constant.

The gas gain for single electrons is scanned by varying the SA voltage while fixing the PA one. The gain can reach up to 3×10^6 as shown in Fig. 3 (right). The gain tested with 5.9 keV X-rays of a ^{55}Fe source is also presented for comparison. A good exponential behavior of the gain over a large range of the working voltage can be observed.

3.2. IBF

During operation, the ions collected on the cathode of the DMM prototype include both the ions produced in the primary ionization and the feedback ones from electron multiplication. The IBF ratio is thus estimated as: $\text{IBF ratio} = (I_{\text{cathode}} - I_{\text{primary}})/I_{\text{anode}}$, where, I_{cathode} is the total current measured from the cathode, I_{primary} is the current from the primary ions, and I_{anode} is the current from the anode. Since I_{primary} is usually much smaller than I_{cathode} , it is ignored in our estimation of IBF ratio.

A Keithley 6482 picoammeter [12] is used to measure all the currents with a resolution of ~ 10 fA at ± 20 nA dynamic range. The test strategy is depicted in Fig. 4 (left). The DMM prototype is operated with the anode at ground when measuring I_{anode} , and the drift cathode at ground when measuring I_{cathode} . This ensured no potential applied on the electrode connected to the picoammeter. The IBF ratio is measured at various total gains by changing the SA voltage, for fixed PA voltages

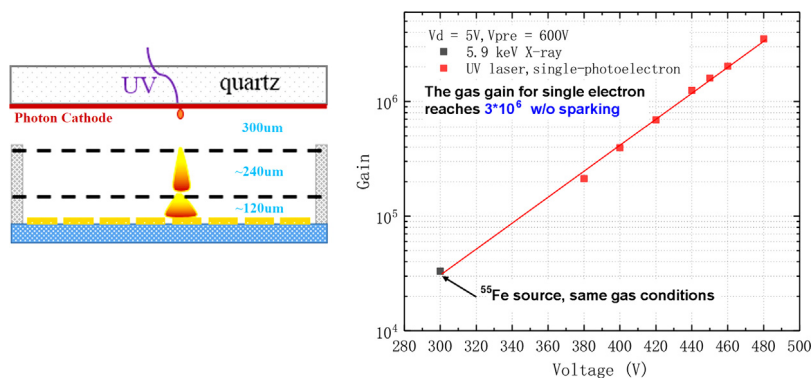


Fig. 3. (left) The schematic configuration of the DMM detector for the laser test. (right) The gas gain for single electrons (red points) and ⁵⁵Fe X-ray events (black point). (For interpretation of the references to color in this figure legend, the reader is referred to the web version of this article.)

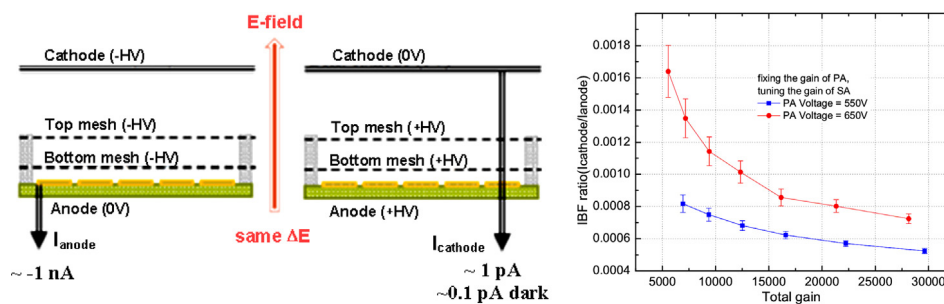


Fig. 4. (left) The IBF ratio test strategy and (right) measured IBF ratios at different total gas gains for two fixed PA voltage settings.

of 550 V and 650 V, respectively. We have checked the IBF measurement at different gains to ensure that the density of ions in drift region is very low, so that the space charge effect can be neglected [13]. As shown in Fig. 4 (right), an IBF ratio of as low as ~ 0.0005 is obtained at a PA voltage of 550 V and a total gain of ~ 30000 . Generally, the IBF ratio decreases with the increasing of SA voltage, and a lower PA voltage helps in with IBF suppression at a same total gain, mainly due to lower PA \rightarrow SA electron transparency at lower E_{PA}/E_{SA} .

In order to better understand the measured low IBF ratio of the DMM prototype, a Garfield++ [14] based simulation study is performed. The electrostatic field in the detector is calculated by the finite element method (FEM) with a simplified geometric structure of DMM, where the braided meshes are replaced with metal plates with arrays of perforations. A low PA \rightarrow SA electron transparency of $\sim 10\%$ level is verified by the simulation, at $E_{PA}/E_{SA} \sim 1$, qualitatively consistent with the experimental result. Furthermore, it is found that the IBF ratio of DMM seriously depends on the geometric alignment of the double meshes. Shown in Fig. 5 are the results of two extreme conditions, where the mesh holes are strictly aligned or the meshes are interlaced (stagger aligned) with minimum optical transparency. In the second case the IBF from the SA region is significantly suppressed by the top mesh, leading to further suppression of the IBF ratio compared to the first case.

According to the simulation, the IBF of the DMM depends on the geometric alignment of the double mesh. Other factors affecting the IBF ratio include gas mixtures, mesh types, thickness of the gaps, etc. Experimental test has been done to check the simulation results. Since it is difficult to align the meshes accurately, a simple attempt is made to tilt an angle between the meshes, as illustrated in Fig. 6 (up), to change the optical transparency of PA \rightarrow SA. The measurements show clear evidence of further IBF suppression. With tilt angles of 15° or 45°, the IBF ratio can reach as low as ~ 0.0003 , shown in Fig. 6 (bottom). Further studies are on-going, with more accurately aligned double meshes.

3.3. Beam test

A similar DMM prototype as in Fig. 3 (left) has been tested with the 150 GeV/c muon beams at CERN. The cathode chosen to be CsI instead of the Chromium in laser test, providing a Cherenkov light yield of ~ 10 photoelectrons. The test is done with the PICOSEC collaboration. In order to get good timing performance, the structure of DMM is tuned to 190 μm (drift) – 120 μm (PA) – 120 μm (SA). The voltages of the PA and SA regions are fixed at 425 V and 360 V. The relative gas gain, IBF ratio and time resolution are scanned by changing the electric field in the drift region. As shown in Fig. 7, the IBF ratio strongly depends on the field setting. The best time resolution can reach 180 ps with an IBF ratio of 0.2%. The variation of gain reflects the co-play of the Drift \rightarrow PA electron transparency and the electron amplification in the drift region.

3.4. Discussions

From the experimental and simulation results presented above, the major factors impacting the IBF ratio can be exploited.

The first main factor is the field ratio E_{PA}/E_D , which not only affects the Drift \rightarrow PA electron transparency, but also significantly limits the ions from drifting back to the drift region from the PA region. The IBF suppression power is roughly E_D/E_{PA} .

The second main factor is the PA \rightarrow SA electron transparency. With similar electric fields in the PA and SA regions, this factor has a similar effect on electrons (PA \rightarrow SA) and ions (SA \rightarrow PA). As demonstrated by the simulation and experiment, the factor gives a suppression power of $\sim 1/10$, which is dependent on the parameters (mesh pitch, expressed in Line Per Inch, optical transparency rate, thickness etc.) of micro-meshes.

The third main factor is the geometric alignment of the double meshes of a DMM, which can be estimated by the overall optical transparency. The mis-alignment of the meshes can efficiently reduce the fraction of IBF, meanwhile has less impact on electron transparency

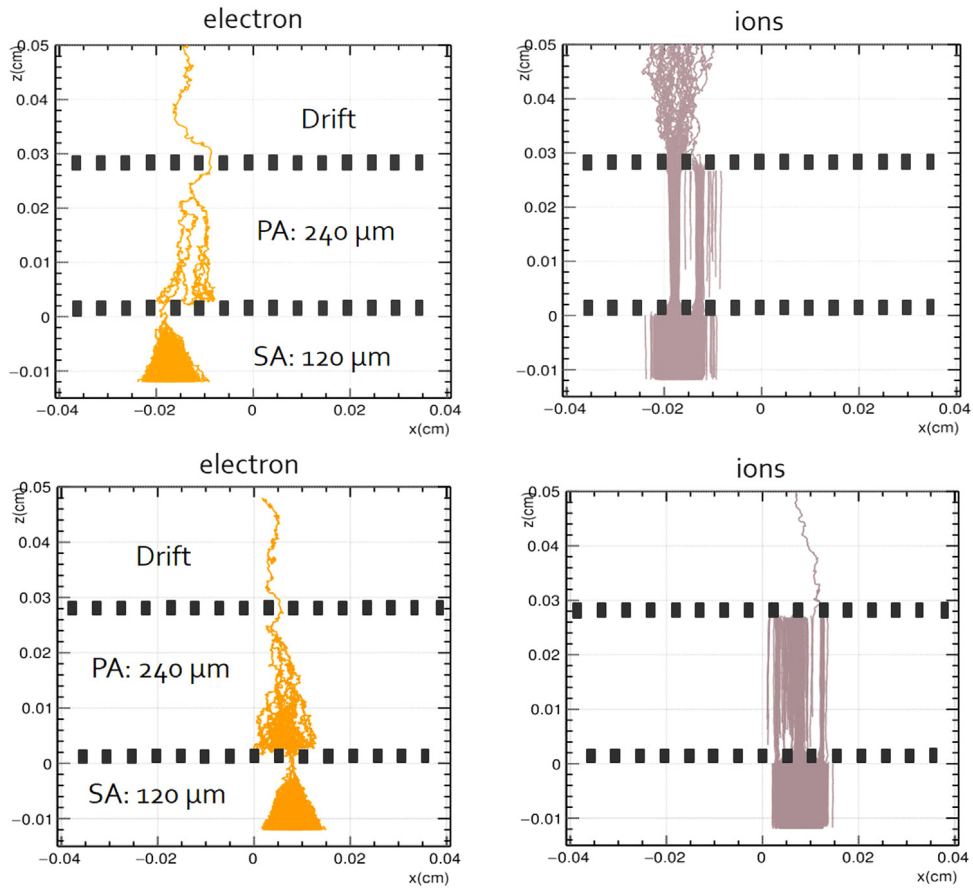


Fig. 5. The simulation results of electron avalanche and charge drifting in a DMM structure. The upper and bottom plots show results of two conditions: mesh holes strictly aligned vs. stagger aligned.

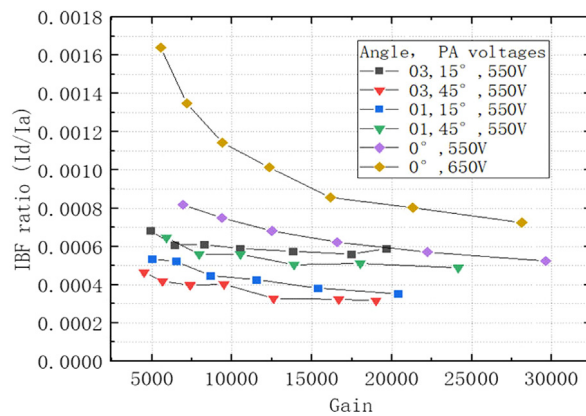
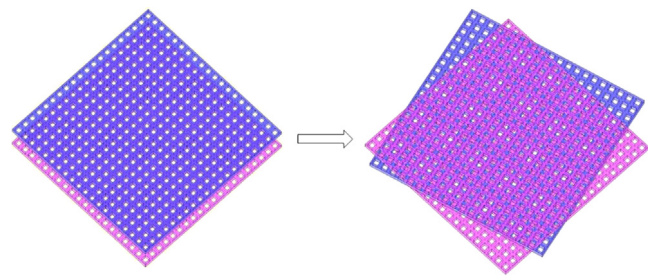


Fig. 6. Further suppression of the IBF ratio with different tilt angles between the double meshes of a DMM.

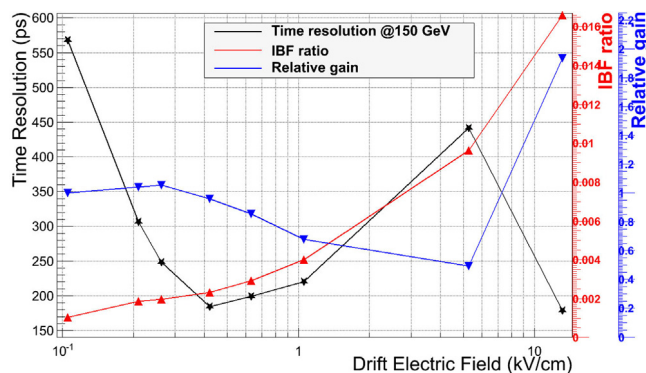


Fig. 7. The beam test results of the relative gas gain, IBF ratio and time resolution as a function of the electric field in the drift region of a DMM.

due to the much larger diffusion effect. This factor may contribute $\sim 1/2 - 1/10$ to the IBF suppression power.

To illustrate the effects of the three main factors, some numerical estimations are given. Starting from 1 electron in the drift region, the total gain can be expressed by $G = G_D \cdot \epsilon_{D \rightarrow PA} \cdot G_{PA} \cdot \epsilon_{PA \rightarrow SA} \cdot G_{SA}$, where $G_D (= 1)$, G_{PA} and G_{SA} are the gain in the drift, PA and SA region; $\epsilon_{D \rightarrow PA}$ and $\epsilon_{PA \rightarrow SA}$ are the electron transparencies from drift to PA and PA to SA region, respectively. The total IBF can also be approximated by $IBF \sim G \cdot \epsilon_{SA \rightarrow PA}^{ion} \cdot f_{Geo} \cdot \epsilon_{PA \rightarrow D}^{ion}$, where $\epsilon_{SA \rightarrow PA}^{ion}$ and $\epsilon_{PA \rightarrow D}^{ion}$ are the ion transparencies from SA to PA and PA to drift, respectively; f_{Geo} is the suppression factor due to geometric alignment.

According to previous discussions in this work, with a similar field in the PA and SA region, we estimate $G_{PA} \sim G_{SA}^2 \sim 10^4$, $\epsilon_{D \rightarrow PA} \sim 1$, $\epsilon_{PA \rightarrow SA} \sim \epsilon_{SA \rightarrow PA}^{ion} \sim 0.1$, $\epsilon_{PA \rightarrow D}^{ion} \sim E_D/E_{PA} \sim 0.01$ and $f_{Geo} \sim 0.1 - 1$ for different possible alignment of meshes. Then the gas gain of such a DMM would be $\sim 10^5$ and the IBF ratio would be $\epsilon_{SA \rightarrow PA}^{ion} \cdot f_{Geo} \cdot \epsilon_{PA \rightarrow D}^{ion} \sim 5 \times 10^{-4}$ for $f_{Geo} \sim 1$ (strict aligned) and 5×10^{-5} for $f_{Geo} \sim 0.1$ (fully mis-aligned).

Summary

A new structure DMM is proposed and the prototype is fabricated and studied with X-ray, UV light and test beam. The features of high gain of $>10^6$ and low IBF ratio of $3-5 \times 10^{-4}$ for the DMM prototype present its great potential for GPM application as well as other applications requiring low IBF ratio. The IBF suppression power of a DMM is discussed, and can be further improved by tuning the drift, PA and

SA voltages, the structural parameters and the optical transparency of the double meshes.

Acknowledgments

This study was supported by National Key Program for S&T Research and Development Grant No. 2016YFA0400400, 2016YFE0104800, the Program of National Natural Science Foundation of China Grant No. 11605197, the Fundamental Research Funds for the Central Universities.

References

- [1] F. Tokanai, et al., Nucl. Instrum. Methods. A 766 (2014) 176–179.
- [2] M. Alexeev, et al., Nucl. Instrum. Methods. A 732 (2013) 264–268.
- [3] K. Matsumoto, et al., Physics Procedia 37 (2012) 499–505.
- [4] D. Attie, et al., JINST 8 (2013) P0519.
- [5] Z.Y. Zhang, et al., Nucl. Instrum. Methods A 889 (2018) 78–82.
- [6] M. Ball, et al., JINST 9 (2014) C04025.
- [7] D.S. Bhattacharya, et al., Nucl. Instrum. Methods. A 861 (2017) 64–70.
- [8] Y.L. Zhang, et al., Chin. Phys. C 41 (5) (2017) 056003.
- [9] L. Guan, et al., Chinese Phys. C 35 (2011) 163.
- [10] Z.Y. Zhang, et al., JINST 9 (2014) C10028.
- [11] COMPILER UPGRADE-400, picosecond lasers, products, <http://passatLtd.com>.
- [12] Keithley series 6400 picoammeter, <https://www.tek.com.cn>.
- [13] P. Colas, et al., Nucl. Instrum. Methods A535 (2004) 226–230.
- [14] <http://garfieldpp.web.cern.ch/garfieldpp/>.